Chemical Physics Letters 694 (2018) 40–47

Contents lists available at ScienceDirect

Chemical Physics Letters

journal homepage: www.elsevier.com/locate/cplett

Research paper

Comparative study of the anchorage and the catalytic properties of nanoporous TiO_2 films modified with ruthenium (II) and rhenium (I) carbonyl complexes

Diego P. Oyarzún [a,*], Sylvie Chardon-Noblat [b], Omar E. Linarez Pérez [c,*], Manuel López Teijelo [c], César Zúñiga [a], Ximena Zarate [d], Eduardo Shott [e], Alexander Carreño [a], Ramiro Arratia-Perez [a]

[a] Center of Applied Nanociences (CANS), Facultad de Ciencias Exactas, Universidad Andres Bello, Chile, Avenida República 275, Santiago, Chile
[b] Université Grenoble Alpes/CNRS, Département de Chimie Moléculaire, UMR 5250, Laboratoire de Chimie Inorganique Redox, BP53, Grenoble 38041 CEDEX 9, France
[c] Instituto de Investigaciones en Fisicoquímica de Córdoba (INFIQC), Facultad de Ciencias Químicas, Universidad Nacional de Córdoba, Haya de la Torre y Medina Allende, 5000 Córdoba, Argentina
[d] Instituto de Ciencias Químicas Aplicadas, Facultad de Ingeniería, Universidad Autónoma de Chile, Av. Pedro de Valdivia 425, Santiago, Chile
[e] Departamento de Química Inorgánica, Facultad de Química, Pontificia Universidad Católica de Chile, Avda. Vicuña Mackenna 4860, Santiago, Chile

ARTICLE INFO

Article history:
Received 5 December 2017
In final form 19 January 2018

Keywords:
Nanoporous TiO_2 films
Ruthenium complex
Rhenium complex
EDS mapping
Catalytic properties

ABSTRACT

In this article we study the anchoring of cis-$[Ru(bpyC_4pyr)(CO)_2(CH_3CN)_2]^{2+}$, cis-$[Ru(bpy)_2(CO)_2]^{2+}$ and cis-$[Ru(bpyac)(CO)_2Cl_2]$, onto nanoporous TiO_2 employing electropolymerization, electrostatic interaction and chemical bonding. Also, the $[Re(bpyac)(CO)_3Cl]$ rhenium(I) complex for chemical anchorage was analyzed. The characterization of TiO_2/Ru(II) and TiO_2/Re(I) nanocomposite films was performed by field emission scanning electron microscopy (FESEM), electron dispersive X-ray spectroscopy (EDS) and Raman spectroscopy. In addition, for the more stable nanocomposites obtained, the catalytic properties (solar energy conversion and CO_2 reduction) were evaluated. The efficiency improvement in redox process derived from the (photo)electrochemical evidence indicates that modified nanoporous TiO_2 structures enhance the rate of charge transfer reactions.

1. Introduction

The photovoltaic cells based on titanium dioxide are well-known for its high-efficiency in dye-sensitized solar cells since Grätzel and co-workers incorporated dinitrogenated ruthenium (II) complexes onto the TiO_2 surface [1–3]. TiO_2 surfaces as rutile or anatase-like forms have a skeleton of titanium and oxygen atoms spatially distributed [4,5] providing a high number of Ti–OH groups on the solid surface [6,7], which allows linking of organometallic compounds and organic chains for the preparation of hybrid materials [8–10]. On the other hand, the controlled manufacture of dye-sensitized TiO_2 structures at the nanometric scale allows either promote or suppress the recombination of electron and hole pairs upon UV–visible light excitation, conferring to TiO_2-based materials an increasing interest within renewable energy and environment fields as well as in nanotechnology [1–5,8,9].

In the last decades, numerous studies have been conducted involving auto-organized nanostructures of different metal oxides and semiconductors, which have received considerable attention due to the potential technological uses of these materials [11,12]. In this way, in order to increase the versatility of the physicochemical properties for different applications, novel modification strategies of nanostructured TiO_2 films have been investigated [13–15].

On the other hand, several reports on the general, flexible and modular ruthenium(II) complexes synthesis of type cis-$Ru(N,N)_2X_2$ (where N,N is a dinitrogenated ligand and X is an halide such as chloride) conclude that the electronic effects produced by the ligands nature and coordination position are fundamental to control their electrochemical properties [16–19]. In addition, numerous studies on electron transfer and transport processes in solar cells based on TiO_2 with ruthenium (II) complexes have demonstrated successful results in energy conversion [16,20]. These findings encourage the development of new methods to immobilize ruthenium-based catalysts onto semiconducting or conducting supports with the purpose of obtaining heterogeneous catalysts. Furthermore, other transition metal complexes such as rhenium compounds have been studied for their photo-

* Corresponding authors.
E-mail addresses: diego.oyarzun@unab.cl (D.P. Oyarzún), olinarez@unc.edu.ar (O.E. Linarez Pérez).

https://doi.org/10.1016/j.cplett.2018.01.040
0009-2614/

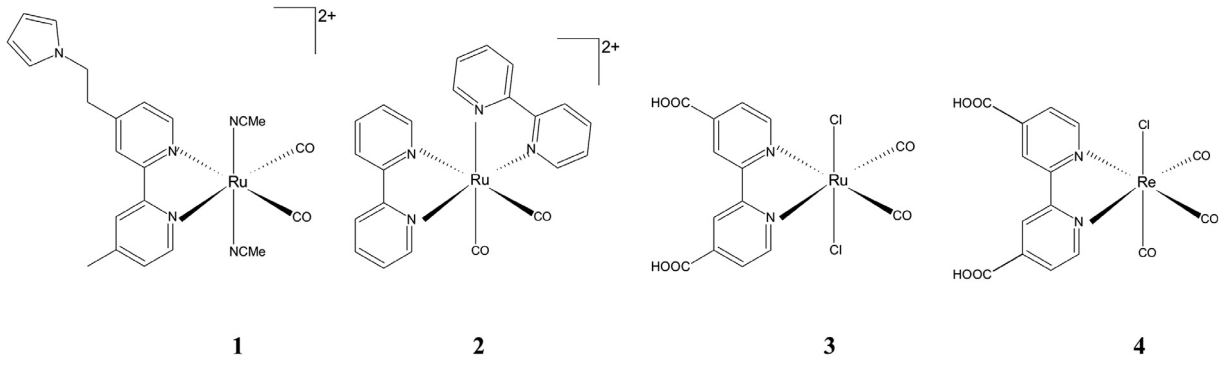

1 2 3 4

Scheme 1. Schematic representation of $[Ru(bpyC_4pyr)(CO)_2(CH_3CN)_2]^{2+}$ (1), $[Ru(bpy)_2(CO)_2]^{2+}$ (2), $[Ru(bpyac)(CO)_2Cl_2]$ (3) and $Re(bpyac)(CO)_3Cl]$ (4) complexes, respectively.

and electrocatalytic properties for the reduction of CO_2 [21–23]. Among several reported compounds, the ruthenium (II) and rhenium (I) complexes harboring carbonyl ligands have promising catalytic properties with the choice of suitable bidentate ligands [24–27]. This type of catalysts could have important applications in new devices for the conversion of CO_2 to value added molecules such as CO, which represent an important technological and environmental challenge [16,21,26,27].

Based on these findings, we carried out the study of nanocomposites based on nanoporous TiO_2 films modified with ruthenium (II) and rhenium (I) complexes (see Scheme 1) by electropolymerization, electrostatic interaction and chemical bonding. The morphologic and chemical characterization of the nanocomposite films obtained for the different anchorage methods is performed by field emission scanning microscopy (FESEM), electron dispersive X-ray spectroscopy (EDS) and Raman spectroscopy. In addition, for the more stable and homogeneous nanocomposite materials obtained, the potential applications in the electroreduction of CO_2 and its applicability as a solar to electrical energy converter by photoelectrochemical methods are evaluated.

2. Experimental

All the starting materials were purchased from Merck and Aldrich and used without further purification. The cis-$[Ru(bpyC_4pyr)(CO)_2(CH_3CN)_2]^{2+}$, cis-$[Ru(bpy)_2(CO)_2]^{2+}$, cis-$[Ru(bpyac)(CO)_2Cl_2]$ and $[Re(bpyac)(CO)_3Cl]$ complexes used in this study were prepared according to literature procedures [28–31]. The anodization of titanium was performed as previously reported [32]. $TiO_2/[Ru(bpyC_4pyr)(CO)_2(CH_3CN)_2]_n$ polymetallic (Ru-Ru) films were grown by continuously cycling the potential between −0.90 and −1.70 V on a TiO_2 nanoporous electrode in a 1 mM solution of $[Ru(bpyC_4Pyr)(CO)_2(CH_3CN)_2]^{2+}$. For the $TiO_2/[Ru(bpy)_2(CO)_2]^{2+}$ modified surface, a previous reduction of the TiO_2 nanoporous electrode by application of a potential pulse at −1.50 V in a solution of CH_3CN + 0.1 M TBAP for 5 min was performed. After that, the ruthenium complex was anchored to the TiO_2 nanoporous film by dipping in a 5 mM of $[Ru(bpy)_2(CO)_2]^{2+}$ in acetonitrile solution for 80 h. Otherwise, prior to the nanoporous TiO_2 surface modification with the $[Ru(bpyac)(CO)_2Cl_2]$ or $[Re(bpyac)(CO)_3Cl]$ complexes, the TiO_2 films was soaked for 1 h in a NaOH aqueous solution (pH 13), copiously washed with water, rinsed with 5 mL of acetonitrile and dried with argon. After that, the catalysts were anchored to the TiO_2 nanoporous films by dipping in a 5 mM of $[Ru(bpyac)(CO)_2Cl_2]$ or $[Re(bpyac)(CO)_3Cl]$ acetonitrile solution for 20, 40, and 80 h.

Electrochemical measurements were made using an EG&G Princeton Applied Research model 273 or 173 potentiostat/galvanostat equipped with a Sefram TGM 164 X–Y recorder. All cyclic voltammograms were obtained in a conventional three-electrode cell under argon or carbon dioxide atmosphere. All potentials reported in organic media are relative to $Ag/AgNO_3$ 10 mM in CH_3CN + 0.1 M TBAP. Supporting electrolyte was n-Bu_4NClO_4 (TBAP) from Fluka. Acetonitrile from Rathburn (HPLC grade) was used as received.

The surface morphology of the modified TiO_2 electrodes was characterized using a Carl Zeiss ∑igma model FESEM microscope. The chemical identification and mapping of the atomic elements in the modified nanoporous TiO_2 films were performed using an EDS spectrometer coupled to the FESEM microscope. Raman experiments were performed ex situ (in air) using a Horiba LabRAM HR spectrometer employing an Ar laser (514.5 nm wavelength). Photoelectrochemical measurements were carried out under solar simulation conditions, employing an UV enhanced Xe lamp of 150 W (Newport Oriel Instruments 6254) mounted in a lamp holder (Oriel 67,005), a water filter (Oriel 61,945) and connected to the cell with a 1 m length optical fiber (Oriel 77,578). A power supply of 40–200 W (Oriel 68,907) was used to generate the arc in the lamp. The illumination power was quantified inside the cell by means of an energy radiant meter (Oriel 70,260). The samples were illuminated at a constant light intensity of 4.0 mW cm^{-2}.

3. Results and discussion

3.1. Preparation and characterization of TiO_2/[M complex] nanocomposites

In order to obtain stable TiO_2/[M complex] nanocomposites for (photo)electrocatalytic investigations, three different ruthenium (**1**–**3**, Scheme 1) and one rhenium (**4**, Scheme 1) coordination complexes were employed. Additionally, according to the chemical nature of the ligands present in the complex molecules, the modification of the nanoporous TiO_2 film was performed by different methods. Furthermore, for the more stable and homogeneous nanocomposites obtained, the chemical characterization by electron dispersive X-ray spectroscopy (EDS) and Raman spectroscopy as well as the photoelectrochemical and electrocatalytic performance are studied.

3.1.1. Electropolymerization

Anodic electropolymerization of the N-functionalized pyrrole (pyr) side of $[Ru(bpyC_4pyr)(CO)_2(CH_3CN)_2]^{2+}$ complex (**1**), is one of the possible ways to modify conductive surfaces [33]. However, for semiconductor materials like TiO_2 nanoporous electrodes, is not possible to carry out the anodic pyr electropolymerization of the complex because of the nanoporous TiO_2 surface does not present enough electronic conductivity in the anodic potential region. For this reason, the anchorage on TiO_2 nanoporous electrodes was

performed by a two-electron irreversible reduction of species **(1)** generating the insoluble $[Ru(bpyC_4pyr)(CO)_2]_n$ organometallic polymer, which is adsorbed on the conductive TiO_2 surface (Eq. (1)) [34].

$$[Ru^{II}(bpyC_4pyr)(CO)_2(CH_3CN)_2]^{2+} + 2e^- \rightarrow [Ru^0(bpyC_4pyr)(CO)_2]_n + 2CH_3CN \quad (1)$$

Fig. 1a shows the potentiodynamic j/E response at 50 mV s^{-1} for successive cycles of a nanoporous TiO_2 film in a 1 mM of (**1**) in CH_3CN + 0.1 M TBAP solution. As the number of cycles increases, an enhancement of the anodic and cathodic current is observed in the −1.40 to −1.10 V region indicating that the electropolymerization takes place, which leads to the deposition of an electroactive polymetallic species onto the TiO_2 surface [34]. Fig. 1b shows the FESEM image of the nanoporous TiO_2 film obtained after the electropolymerization process. A cloudy and non-homogeneous morphology of the deposit at the nanoporous TiO_2 film surface is observed. The cathodic electropolymerization of the organometallic complex is very disordered and the polymetallic deposit covers completely the surface of TiO_2 nanoporous electrode diminishing the original large surface area of the substrate. In addition, the poly-Ru polymer proved to be very unstable and, in contact with air, the Ru^0 metal centers are oxidized leading to soluble Ru^{II} monomer species (Eq. (2)) [31].

$$[Ru^0(bpyC_4pyr)(CO)_2]_n \rightarrow n[Ru^{II}(bpyC_4pyr)(CO)_2X_2]^{2+} + 2ne^- \quad (2)$$

Fig. 1c shows comparatively the CV response at 50 mV s^{-1} for a transferred $TiO_2/[Ru(bpyC_4pyr)(CO)_2(CH_3CN)_2]_n$ nanocomposite and the as-prepared TiO_2 nanoporous film to a 0.1 M TBAP in CH_3CN solution. An increase of the reduction current at around −1.50 V for the nanocomposite material is obtained, which is attributed to the redox properties of the ruthenium metal centers that were spontaneously obtained by oxidation in contact with air in the proximity of the electrode surface prior to the electrochemical measurement. Therefore, because of the loss of electroactive Ru polymetallic compound by oxidation in air, it can be concluded that this composite is not suitable for possible further applications.

3.1.2. Electrostatic anchorage

As the TiO_2/[Ru] nanocomposite preparation by cathodic electropolymerization of the pyrrole functionalized ruthenium complex (**1** in Scheme 1) leads to an unstable modified surface, another anchorage method, i.e. dipping of the substrate in ruthenium complex solutions has been tested. For this purpose, $[Ru(bpy)_2(CO)_2]^{2+}$ complex (**2** in Scheme 1) was investigated. As **2** is a positively charged species, the electrostatic interaction with a negative surface may be used as anchorage method. In order to obtain negatively charged substrates, the nanotubular TiO_2 surfaces were electroreduced by application of a potential pulse at −1.50 V for 5 min in a 0.1 M TBAP in CH_3CN solution prior to the dipping. It is well-known that this procedure generates TiO_2 (e^-) species at the base of the pores and the resultant blue-black-colored substrate is stable in the absence of O_2 or other electron acceptors [35].

Fig. 2a shows the potentiodynamic j/E response for a $TiO_2/[Ru(bpy)_2(CO)_2]^{2+}$ nanocomposite obtained after 80 h of dipping as compared with the response of the as-prepared nanoporous TiO_2 film. The FESEM image of the nanocomposite obtained is also shown in Fig. 2b. Even for long dipping times (80 h), no noticeable modification in the current profile or in the surface morphology was obtained. In conclusion, neither the ruthenium complex **2** nor the procedure employed for the nanocomposite preparation, are appropriate for electrocatalytic applications.

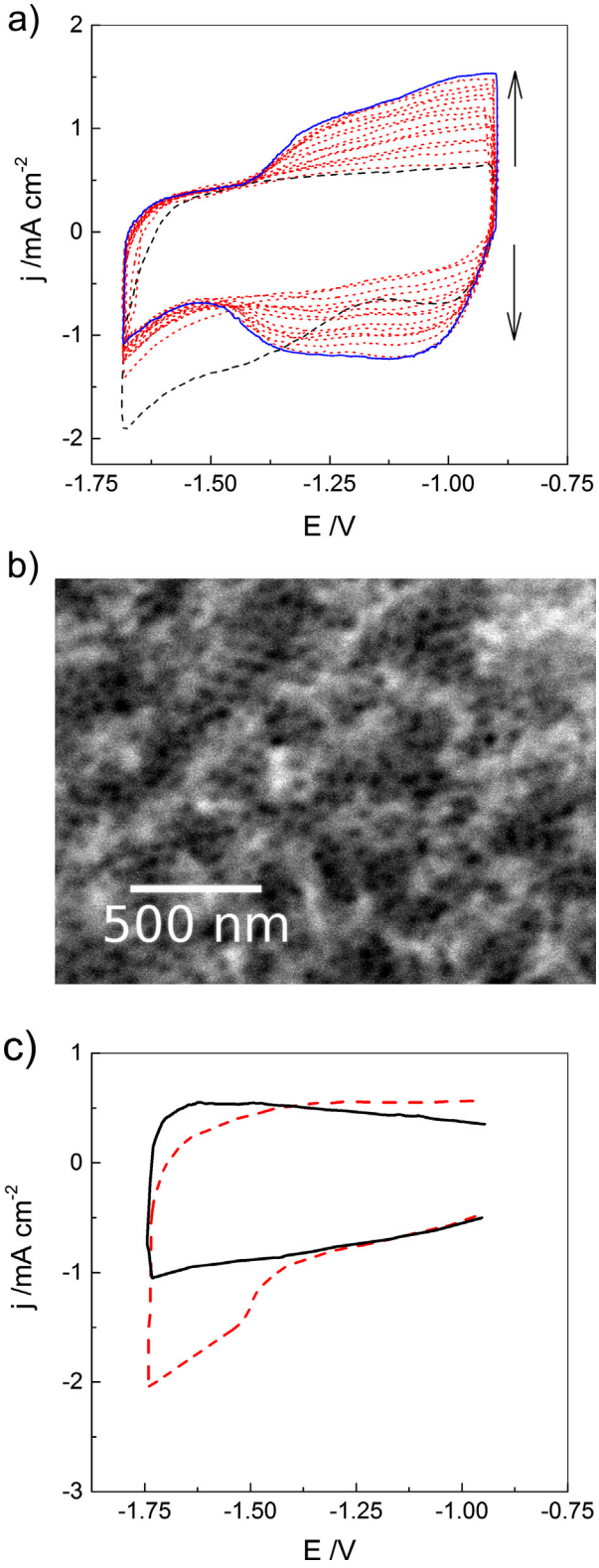

Fig. 1. (a) Potentiodynamic j/E response at 50 mV s^{-1} for electrochemical generation of the organometallic polymer on TiO_2 nanoporous electrode in 1 mM $[Ru(bpyC_4pyr)(CO)_2(CH_3CN)_2]^{2+}$ in CH_3CN + 0.1 M TBAP solution. Arrows indicate increasing cycle's number from the 1st cycle (black dashed line) to the 16th cycle (blue continuous line). (b) FESEM image for the $TiO_2/[Ru(bpyC_4pyr)(CO)_2]_n$ nanocomposite obtained. (c) Potentiodynamic j/E response at 50 mV s^{-1} for nanoporous TiO_2 (continuous line) and $TiO_2/[Ru(bpyC_4pyr)(CO)_2(CH_3CN)_2]_n$ modified electrodes (red dashed line) in a 0.1 M TBAP in CH_3CN solution. (For interpretation of the references to colour in this figure legend, the reader is referred to the web version of this article.)

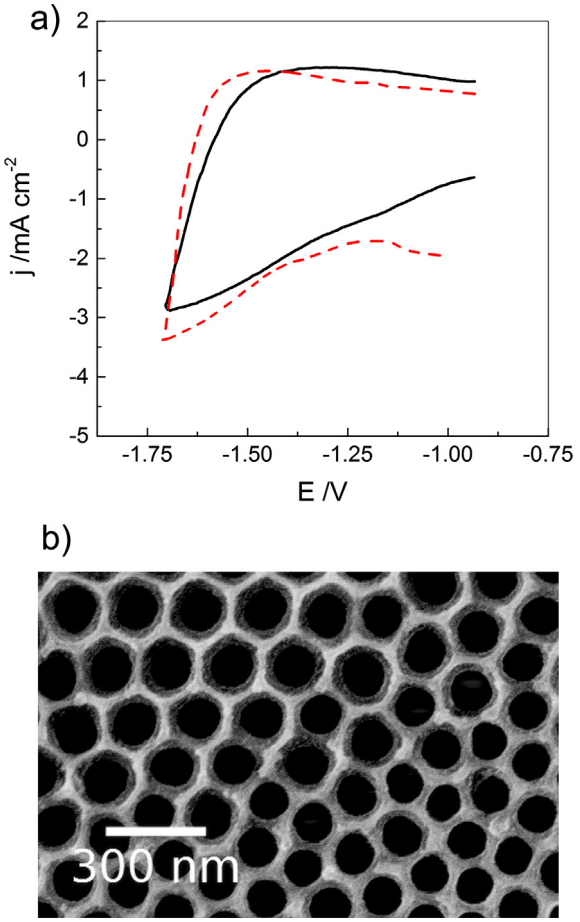

Fig. 2. (a) Potentiodynamic j/E response at 50 mV s^{-1} in CH_3CN + 0.1 M TBAP for nanoporous TiO_2 film (continuous line) and a TiO_2/$[Ru(bpy)_2(CO)_2]^{2+}$ modified electrode (red dashed line) obtained after 80 h dipping in a 2.5 mM solution of complex 2. (b) FESEM image of the modified electrode surface. (For interpretation of the references to colour in this figure legend, the reader is referred to the web version of this article.)

3.1.3. Chemical anchorage

As an alternative for nanocomposites preparation by the dipping method, both ruthenium complex **3** and rhenium complex **4** were employed. Prior to dipping, the nanoporous TiO_2 films were pretreated with an 0.1 M NaOH aqueous solution (pH 13) in order to promote the formation of terminal hydroxyl groups on the TiO_2 surface (>Ti-OH) and thus favoring the chemical anchorage of the complex via an esterification reaction between the surface hydroxyl groups and the carboxylic acid groups of the ligands [36,37].

Fig. 3a shows the CVs response of TiO_2/$[Ru(bpyac)(CO)_2Cl_2]$ nanocomposite electrodes in CH_3CN + 0.1 M TBAP, prepared for different dipping times up to 80 h in a 5 mM of **3** in acetonitrile solution compared with those obtained for net nanoporous TiO_2 film in a CH_3CN + 0.1 M TBAP solution. This response exposes two quasi-reversible systems. The first system, at ca. −1.0 V, corresponds to the reduction/oxidation of the metal in the film, while the second one, at −1.5 V, is attributed to the reduction of the ligand bpy to $bpy^{\cdot-}$ [38]. As the dipping time is increased up to 40 h, an enhancement of the anodic and cathodic currents is observed. For higher dipping times, nearly the same current profile is obtained indicating that maximum coverage of the nanoporous TiO_2 films with the ruthenium complex has been reached. Because of the high aspect ratio of the TiO_2 nanopores (8.74 μm length/around 120 nm diameter [39]), the complex species would need a time higher than 20 h in order to penetrate into the pores and then saturate the nanocomposite structure.

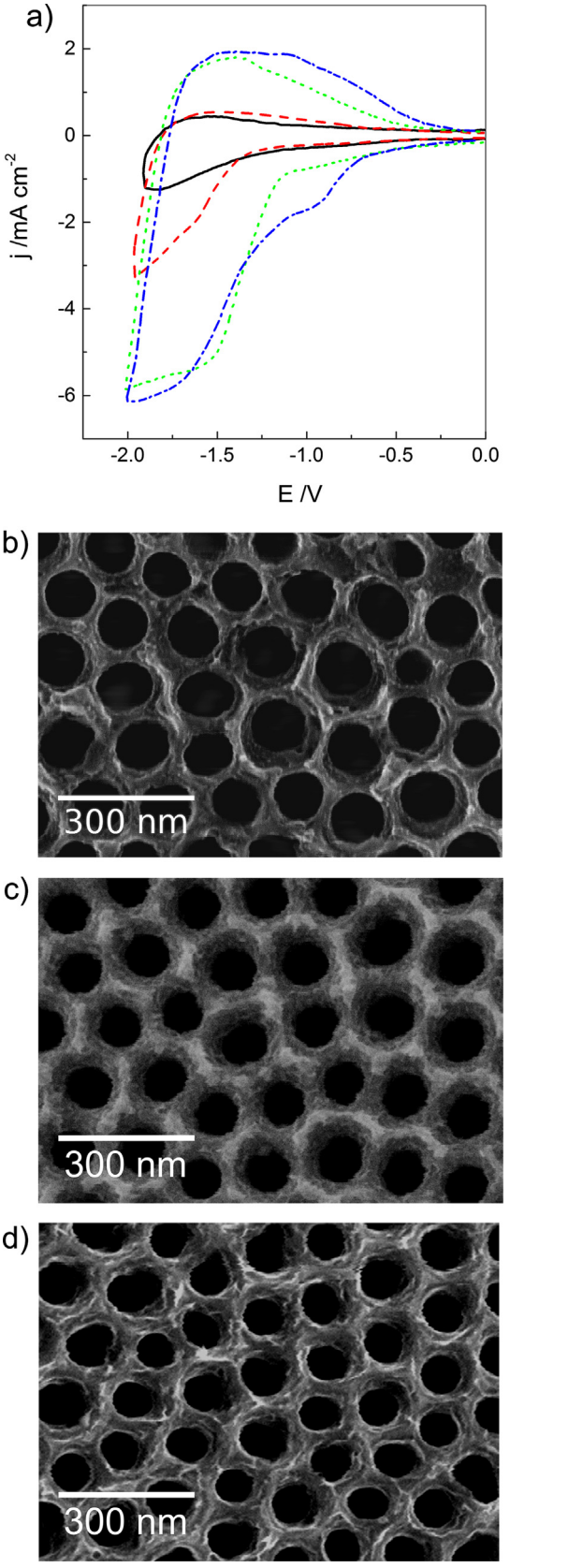

Fig. 3. (a) Potentiodynamic j/E response at 50 mV s^{-1} for nanoporous TiO_2 film (continuous line) and TiO_2/$[Ru(bpyac)(CO)_2Cl_2]$ modified electrodes obtained for different dipping times in CH_3CN + 0.1 M TBAP: 20 h (– – –), 40 h (·····) and 80 h (–·–·–). (b–d) FESEM images for a nanoporous TiO_2 film (b), TiO_2/$[Ru(bpyac)(CO)_2Cl_2]$ (c) and TiO_2/$[Re(bpyac)(CO)_3Cl]$ (d) modified surfaces for 40 h dipping time.

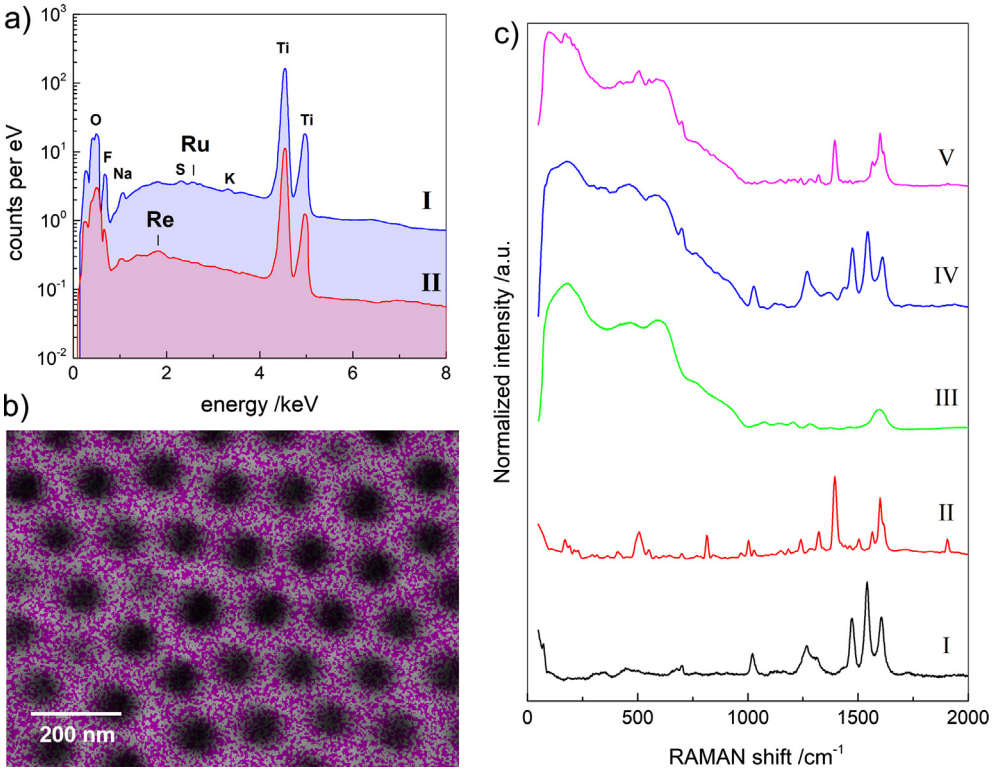

Fig. 4. (a) EDS spectrum taken to an energy of 20 keV (shown up to 8 keV) for TiO_2/[Ru(bpyac)$(CO)_2Cl_2$] (I) and TiO_2/[Re(bpyac)$(CO)_3$Cl] (II) modified surfaces. (b) 1.00 × 0.75 μm^2 EDS mapping image for the Ru Lα line (2.558 keV) on TiO_2 nanoporous film (dark magenta pixels). (c) RAMAN spectra of solid [Ru(bpyac)$(CO)_2Cl_2$] (I), solid [Re(bpyac)$(CO)_3$Cl] (II), TiO_2 nanoporous surface (III), TiO_2/[Ru(bpyac)$(CO)_2Cl_2$] modified surface (IV) and TiO_2/[Re(bpyac)$(CO)_3$Cl] modified surface (V). (For interpretation of the references to colour in this figure legend, the reader is referred to the web version of this article.)

Fig. 3b–d show FESEM images of a nanoporous TiO_2 film (Fig. 3b) and TiO_2/[Ru(bpyac)$(CO)_2Cl_2$] (Fig. 3c) or TiO_2/[Re(bpyac)$(CO)_3$Cl] (Fig. 3d) nanocomposites obtained after 40 h dipping in a 5 mM of **3** or **4** in acetonitrile solution. After the dipping, different contrast and outward appearance are observed in the images due to the surface modification.

In order to determine the presence of the ruthenium (**3**) and rhenium (**4**) complexes in the TiO_2/[M] nanocomposites as well as the molecular interactions taking place, a qualitative EDS chemical analysis and Raman measurements were performed. Fig. 4a shows the 20 keV EDS spectrum for TiO_2/[Ru(bpyac)$(CO)_2Cl_2$] and TiO_2/[Re(bpyac)$(CO)_3$Cl] nanocomposites in the 0–8 keV energy range. For both nanocomposites, well-defined and intense signals for Ti Kα (4.508 keV), Ti Kβ (4.931 keV) as well as O Kα (0.525 keV) due to the titanium substrate and the TiO_2 film, are obtained. Additionally, as the nanoporous TiO_2 films were prepared in fluoride-containing electrolytes, the F Kα (0.677 keV) line obtained indicates the incorporation of fluoride ions in the films during the synthesis, as previously reported [32]. Furthermore, the weak signals appearing at 2.558 keV (Ru Lα line) and 1.842 keV (Re M line), indicate the presence of ruthenium and rhenium complexes on both modified TiO_2 surfaces. Other minority signals superimposed upon the background of continuum X-rays that correspond to trace contaminants (Na, K, S), are also obtained. Complementarily, an EDS mapping collecting the Ru Lα line counts for the TiO_2/[Ru(bpyac)$(CO)_2Cl_2$] was performed. Fig. 4b shows a 1.00 × 0.75 μm^2 EDS mapping image overlapped to the corresponding secondary-electron image. A homogeneous distribution of the ruthenium signal at the surface is obtained, which indicates a high coverage of the [Ru(bpyac)$(CO)_2Cl_2$] complex at the nanoporous TiO_2 film.

Fig. 4c shows the Raman spectra obtained for the solid [Ru(bpyac)$(CO)_2Cl_2$] **(I)** and [Re(bpyac)$(CO)_3$Cl] **(II)** complexes, the TiO_2 unmodified nanoporous surface **(III)** and the TiO_2/[Ru(bpyac)$(CO)_2Cl_2$] **(IV)** or TiO_2/[Re(bpyac)$(CO)_3$Cl] **(V)** modified surfaces. For the solid dyes (Fig. 4c-I and c-II), mainly the 2,2′-bipyridine-4,4′-dicarboxylic acid ligand (bpyac) characteristic vibrations are obtained, namely the ring breathing at 1021.1 cm^{-1}; the C–C–H in-plane bend at 1265 cm^{-1}; the C–C inter-ring stretching at 1318 cm^{-1}; and those corresponding to C–C, C–N and C–O stretchings at 1472, 1541.4 and 1606.1 cm^{-1}, respectively [40]. For nanoporous TiO_2 films (Fig. 4c-III), the presence of broad bands at 187; 464 and 606 cm^{-1} and the absence of well-defined signals corresponding to anatase (144; 399; 515 and 640 cm^{-1}) or rutile (240; 447 and 612 cm^{-1}) crystalline phases, indicate that the anodic films obtained are amorphous [41]. On the other hand, for the modified TiO_2 surfaces (Fig. 4c-IV and c-V), the overlapping of the porous TiO_2 [41] (Fig. 4c-III) and the ruthenium (Fig. 4c-I) or rhenium (Fig. 4c-II) complexes Raman signals is obtained. For energies higher than 700 cm^{-1}, the bands in the spectra are similar in position and relative intensity to those obtained for the solid dyes (Fig. 4c-I and II) indicating the presence of either [Ru(bpyac)$(CO)_2Cl_2$] or [Re(bpyac)$(CO)_3$Cl] complexes. Additionally, in comparison to the spectrum of the solid dyes, the presence of a new peak at around 700 cm^{-1} indicates that the complex molecules are linked to the hydroxylated TiO_2 surface by the esterification of the carboxylate groups at the position 4 in the pyridine rings of the bipyridile ligands [42].

3.2. Photocatalytic study

In order to analyze the photoelectrochemical behavior of the nanocomposites for further applications, potentiostatic photocurrent measurements in aqueous solution were performed. Fig. 5 shows the photocurrent transients recorded at different constant potentials for the nanoporous TiO_2 substrate (Fig. 5a) and TiO_2/[Re(bpyac)$(CO)_3$Cl] (Fig. 5b) or TiO_2/[Ru(bpyac)$(CO)_2Cl_2$] (Fig. 5c) nanocomposites. For all the substrates, the squared-

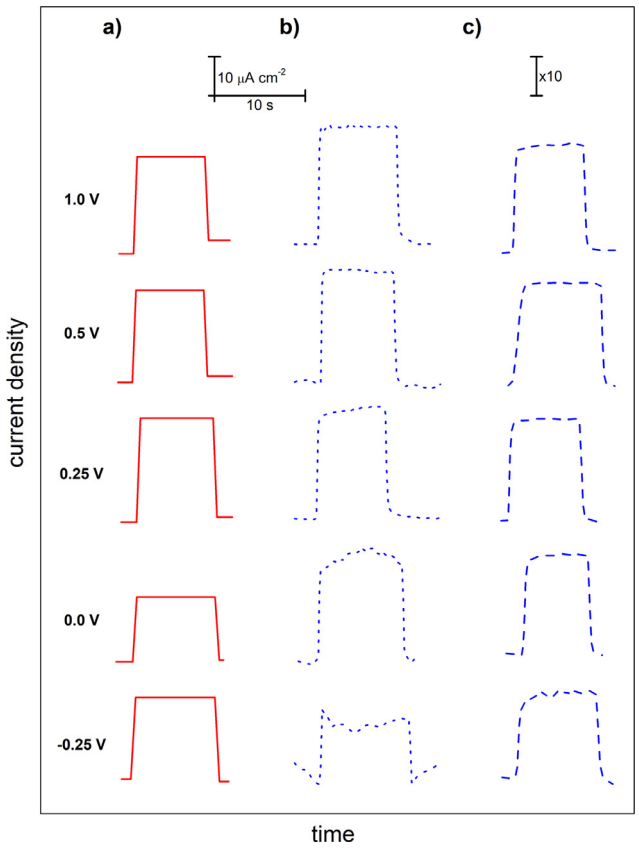

Fig. 5. Potentiostatic j/t photocurrent transients obtained at different potentials for nanoporous TiO_2 films (a), and TiO_2/[Re(bpyac)$(CO)_3$Cl] (b), TiO_2/[Ru(bpyac)$(CO)_2Cl_2$] (c) modified electrodes.

shape of the transients obtained indicates that the recombination process may not occur at a significant rate. In addition, after illumination starts, the photocurrent reaches the steady value ($j_{Ph,st}$) indicating that all the photogenerated charges are being used in a process of faradaic nature [32]. For the nanoporous TiO_2/electrolyte system (Fig. 5a), insignificant differences between photocurrent values (~25 μA cm^{-2}) obtained for the different potentials applied indicate that an increase in the curvature of the bands does not improve the separation of the charge carriers for the faradaic process. Additionally, only a slight increase in the photocurrent response for the TiO_2/[Re(bpyac)$(CO)_3$Cl] nanocomposite (Fig. 5b) is obtained. Contrarily, for the TiO_2 nanoporous electrode modified with [Ru(bpyac)$(CO)_2Cl_2$] (Fig. 5c; please note the ×10 increase in the current scale), the stationary photocurrent $j_{Ph,st}$ increases about 10-times for all potential values applied, indicating that this nanocomposite system has a much better performance for the oxidation process in comparison with the non-modified or rhenium modified TiO_2 nanoporous films. This behavior can be attributed to the higher visible adsorption cross-section of the ruthenium complexes and a better accumulation of the photogenerated charge carriers in the space charge region into the TiO_2 film, which are later separated by the applied electric field.

3.3. Electrocatalytic reduction of CO_2

It is well-known that the electrochemical reduction of CO_2 under appropriate conditions can lead to the synthesis of organic compounds, i.e. alcohols, alkanes. Bare or modified gold, copper or platinum surfaces have shown to be attractive electrode materials for synthetic production of carbon-based chemicals [30,43,44], although the main drawback of these metallic catalysts is the low selectivity and efficiency. In this context, the electroreduction of CO_2 using TiO_2/[Ru(bpyac)$(CO)_2Cl_2$] and TiO_2/[Re(bpyac)$(CO)_3$Cl] nanocomposites as electrode was studied.

Fig. 6 shows the potentiodynamic j/E response in either Ar- or CO_2-saturated acetonitrile solutions at atmospheric pressure for TiO_2/[Ru(bpyac)$(CO)_2Cl_2$] (Fig. 6a) and TiO_2/[Re(bpyac)$(CO)_3$Cl] (Fig. 6b) nanocomposites obtained after 40 h of dipping. For both complexes, in the presence of CO_2 the j/E curves show an increase in the cathodic current over the entire potential range covered, which may be associated with CO_2 reduction. However, it is important to note that higher cathodic current values for the TiO_2/[Ru(bpyac)$(CO)_2Cl_2$] nanocomposite are obtained, which is associated with the catalytic reduction of CO_2. Additionally, for this composite electrode the reduction processes are observed at potentials much lower than that obtained for the rhenium complex, being a clear indication that TiO_2/[Ru(bpyac)$(CO)_2Cl_2$] is a better electrocatalyst for CO_2 reduction. Nevertheless, further studies are needed both in the preparation and in the analysis of

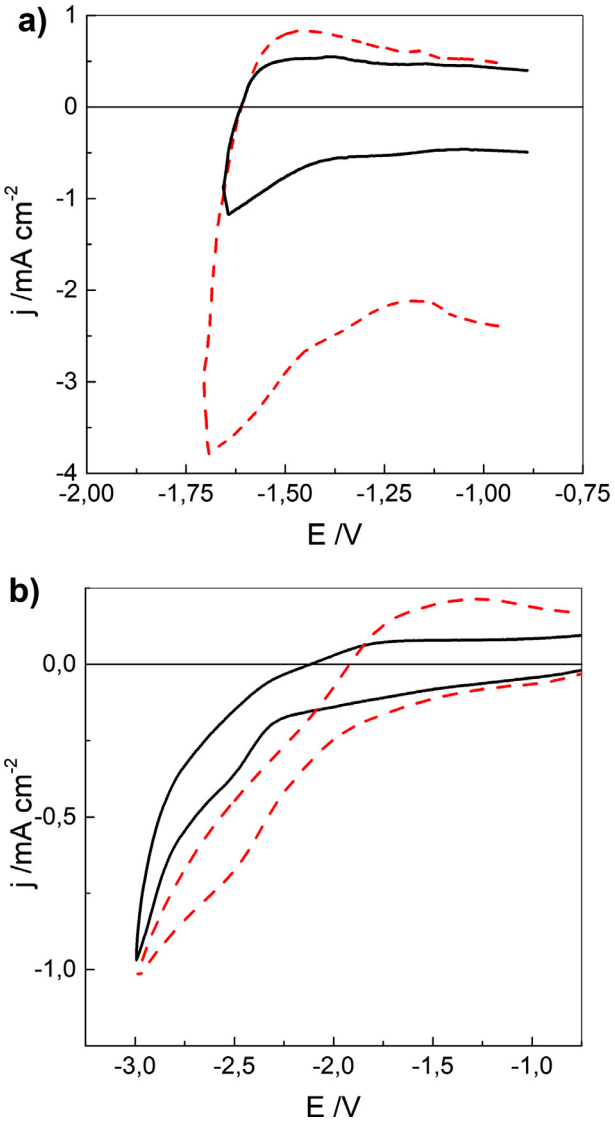

Fig. 6. Potentiodynamic j/E response at 50 mV s^{-1} for TiO_2/[Ru(bpyac)$(CO)_2Cl_2$] (a) and TiO_2/[Re(bpyac)$(CO)_3$Cl] (b) electrodes in CH_3CN + 0.1 M TBAP recorded under argon atmosphere (continuous lines) or under CO_2 atmosphere (dashed lines).

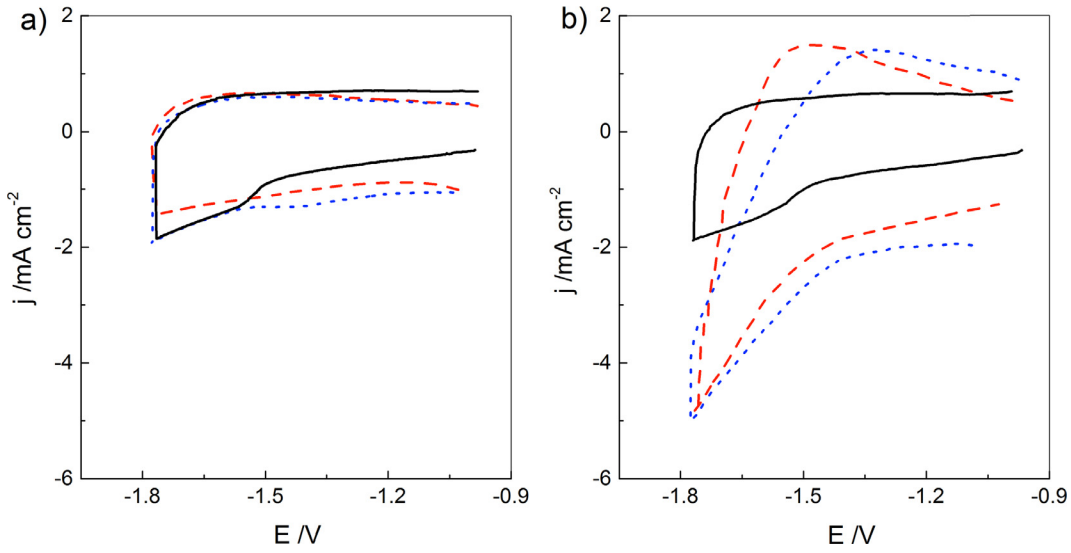

Fig. 7. Potentiodynamic j/E response at 50 mV s^{-1} for TiO_2/[Ru(bpyac)$(CO)_2Cl_2$] modified electrodes under Ar (a) or CO_2 (b) atmosphere in CH_3CN + 0.1 M TBAP with different water content: 0% (——); 1% (– – –) and 5% (·····).

properties in order to improve the performance of the nanocomposites.

It is also known that for classical modified electrodes, addition of water produces an increase in the reduction rate since participates, through protonation steps, in the mechanism suggested for electrocatalytic reduction of CO_2 [34]. Fig. 7 shows the potentiodynamic j/E response recorded for TiO_2/[Ru(bpyac)$(CO)_2Cl_2$] nanocomposites obtained after 40 h of dipping in either Ar- or CO_2- saturated acetonitrile solutions with the addition of different quantities of water. For experiments under Ar atmosphere (Fig. 7a), as the water content increases no evident changes in the current profiles are observed indicating that no additional charge transfer reaction takes place, while in the presence of CO_2, the progressive addition of water to the electrolyte produces a marked increase in the CO_2 reduction current (Fig. 7b), that may be associated to catalytic reduction of CO_2. For the present experimental conditions, the maximum effect on the reduction current is reached for an amount of 1% water (Fig. 7b). These findings are in full agreement with previously reported catalytic cycles [34].

4. Conclusions

In the present work, cis-[Ru(bpyC_4pyr)$(CO)_2(CH_3CN)_2]^{2+}$, cis-[Ru(bpy$)_2(CO)_2]^{2+}$, cis-[Ru(bpyac)$(CO)_2Cl_2$] and [Re(bpyac)$(CO)_3$Cl] complexes harboring carbonyl ligands were anchored onto nanoporous TiO_2 films. The TiO_2/[M] nanocomposites showed to be chemically stable when they are chemically linked to the TiO_2 nanoporous film, producing homogeneous layers with large surface area. The more efficient anchorage for nanocomposites based on ruthenium (II) or rhenium (I) complexes in our study were those complex species that present carboxylate groups as substituent in the dinitrogenated ligand. The TiO_2 surface modification takes place by chemical bonding (Fisher esterification) between carboxylate groups with surface -OH groups on the TiO_2 matrix. Long dipping times are needed (>40 h) in order to obtain the maximum coverage of the surface due to the high aspect ratio or the nanoporous TiO_2 films. The findings indicate that the TiO_2/[Ru] nanocomposites generated present interesting performance in terms of the photocurrent obtained for the oxidation process observed, which can be attributed to the charge carriers that were photogenerated and accumulated in the space charge region. Later, the photogenerated electron–hole pairs are separated by the electric field applied in the space charge layer. The shifting of the applied potential to less negative values does not improve significantly the photocurrent performance.

The electrocatalytical activity of TiO_2/[Ru(bpyac)$(CO)_2Cl_2$] as well as TiO_2/[Re(bpyac)$(CO)_3$Cl] nanocomposites for the reduction of CO_2 was evaluated. The evidence shows that the modified TiO_2 nanoporous films improve the reduction charge transfer reactions because of the high surface area improving the electrocatalytic properties of the semiconductor substrate. These findings indicate that the nanocomposites generated are suitable candidates in the design of new materials for (photo)electrocatalytical applications.

Acknowledgements

We thank to project PMI–CD InES of Universidad Andrés Bello for the financial support for this study, to the Iniciativa Científica Milenio (ICM) del Ministerio de Economía, Fomento y Turismo del Gobierno de Chile and DAAD PUCV to stay for funding the research at the Université Grenoble Alpes / CNRS. OELP and MLT thank the financial support from CONICET, ANPCYT and SECYT-UNC. FESEM and EDS mapping facilities at LAMARX and Raman facilities at "Laboratorio de Nanoscopia y Nanofotónica – LANN", INFIQC–CONICET/UNC, "Sistema Nacional de Microscopía", MINCyT, are gratefully acknowledged. FONDECYT 1161416, 11140563 and 11170637.

References

[1] B. O'Regan, M. Grätzel, A low-cost, high-efficiency solar cell based on dye-sensitized colloidal TiO_2 films, Nature 353 (1991) 737–740.
[2] Md.K. Nazeeruddin, S.M. Zakeeruddin, R. Humphry-Baker, M. Jirousek, P. Liska, N. Vlachopoulos, V. Shklover, C.-H. Fischer, M. Grätzel, Acid–base equilibria of (2,2′-Bipyridyl-4,4′-dicarboxylic acid)ruthenium(II) complexes and the effect of protonation on charge-transfer sensitization of nanocrystalline titania, Inorg. Chem. 38 (1999) 6298–6305.
[3] O. Kohle, S. Ruile, M. Grätzel, Ruthenium(II) charge-transfer sensitizers containing 4,4′-Dicarboxy-2,2′-bipyridine. Synthesis, properties, and bonding mode of coordinated thio- and selenocyanates, Inorg. Chem. 35 (1996) 4779–4787.
[4] M. Dahl, Y. Liu, Y. Yin, Composite titanium dioxide nanomaterials, Chem. Rev. 114 (2014) 9853–9889.
[5] M.T. Brumbach, A.K. Boal, D.R. Wheeler, Metalloporphyrin assemblies on pyridine-functionalized titanium dioxide, Langmuir 25 (2009) 10685–10690.
[6] S. Gawęda, G. Stochel, K. Szaciłowski, Photosensitization and photocurrent switching in carminic acid/titanium dioxide hybrid material, J. Phys. Chem. C 112 (2008) 19131–19141.

[7] M. Aryanpour, R. Hoffmann, F.J. DiSalvo, Tungsten-doped titanium dioxide in the rutile structure: theoretical considerations, Chem. Mater. 21 (2009) 1627–1635.
[8] M. Shakir, N. Iram, M. Shoeb Khan, S.I. Al-Resayes, A. Ali Khan, U. Baig, Electrical conductivity, isothermal stability, and ammonia-sensing performance of newly synthesized and characterized organic-inorganic polycarbazole–titanium dioxide nanocomposite, Ind. Eng. Chem. Res. 53 (2014) 8035–8044.
[9] Z. Sun, L. Xu, W. Guo, B. Xu, S. Liu, F. Li, Enhanced photoelectrochemical performance of nanocomposite film fabricated by self-assembly of titanium dioxide and polyoxometalates, J. Phys. Chem. C 114 (2010) 5211–5216.
[10] K. Milowska, A. Rybczynska, J. Mosiolek, J. Durdyn, E.M. Szewczyk, N. Katir, Y. Brahmi, J.P. Majoral, M. Bousmina, M. Bryszewska, A. El Kadib, Biological activity of mesoporous dendrimer-coated titanium dioxide: insight on the role of the surface-interface composition and the framework crystallinity, ACS Appl. Mater. Interfaces 7 (2015) 19994–20003.
[11] S. Sung, S. Park, W.J. Lee, J. Son, C.H. Kim, Y. Kim, D.Y. Noh, M.H. Yoon, Low-voltage flexible organic electronics based on high-performance sol-gel titanium dioxide dielectric, ACS Appl. Mater. Interfaces 7 (2015) 7456–7461.
[12] A.V. Agafonov, O.I. Davydova, A.S. Krayev, O.S. Ivanova, O.L. Evdokimova, T.V. Gerasimova, A.E. Baranchikov, V.V. Kozik, V.K. Ivanov, Unexpected effects of activator molecules' polarity on the electroreological activity of titanium dioxide nanopowders, J. Phys. Chem. B 121 (2017) 6732–6738.
[13] D. Koch, S. Manzhos, On the charge state of titanium in titanium dioxide, J. Phys. Chem. Lett. 8 (2017) 1593–1598.
[14] F. Kuralay, S. Tunç, F. Bozduman, L. Oksuz, A.U. Oksuz, Biosensing applications of titanium dioxide coated graphene modified disposable electrodes, Talanta 160 (2016) 325–331.
[15] C. Evangelisti, M. Guidotti, C. Tiozzo, R. Psaro, N. Maksimchuk, I. Ivanchikova, A.N. Shmakov, O. Kholdeeva, Titanium-silica catalyst derived from defined metallic titanium cluster precursor: synthesis and catalytic properties in selective oxidations, Inorgan. Chim. Acta 470 (2018) 393–401.
[16] K. Singha, P. Laha, F. Chandra, N. Dehury, A.L. Koner, S. Patra, Long-lived polypyridyl based mononuclear ruthenium complexes: synthesis, structure, and azo dye decomposition, Inorg. Chem. 56 (2017) 6489–6498.
[17] M.G. Mellace, F. Fagalde, N.E. Katz, I.G. Crivelli, A. Delgadillo, A.M. Leiva, B. Loeb, M.T. Garland, R. Baggio, Dinuclear asymmetric ruthenium complexes with 5-cyano-1,10-phenanthroline as a bridging ligand, Inorg. Chem. 43 (2004) 1100–1107.
[18] S. Kamalesu, K. Swarnalatha, R. Subramanian, K. Muralidharan, S. Gomathi, Polypyridyl-hydrazone based Ruthenium(II) complexes: Spectral and computational analysis, Inorganica Chim. Acta 461 (2017) 35–44.
[19] S.E. Domínguez, F. Fagalde, Electrochemical disproportionation in new ruthenium (II) nitro complexes with 2,4,6-tris(2-pyridyl)-1,3,5-triazine detected by IR spectroelectrochemistry with an OTTLE cell, Inorg. Chem. Commun. 77 (2017) 31–34.
[20] W.C. Chen, F.T. Kong, Z.Q. Li, J.H. Pan, X.P. Liu, F.L. Guo, L. Zhou, Y. Huang, T. Yu, S.Y. Dai, Superior light-harvesting heteroleptic ruthenium(ii) complexes with electron-donating antennas for high performance dye-sensitized solar cells, ACS Appl. Mater. Interfaces 8 (2016) 19410–19417.
[21] Y. Kuninobu, K. Takai, Organic reactions catalyzed by rhenium carbonyl complexes, Chem. Rev. 111 (2011) 1938–1953.
[22] C.W. Machan, S.A. Chabolla, C.P. Kubiak, Reductive disproportionation of carbon dioxide by an alkyl-functionalized pyridine monoimine Re(I) *fac*-tricarbonyl electrocatalyst, Organometallics 34 (2015) 4678–4683.
[23] G. Valenti, M. Panigati, A. Boni, G. D'Alfonso, F. Paolucci, L. Prodi, Diazine bridged dinuclear rhenium complex: new molecular material for the CO_2 conversion, Inorganica Chim. Acta 417 (2014) 270–273.
[24] W.H. Wang, Y. Himeda, J.T. Muckerman, G.F. Manbeck, E. Fujita, CO_2 hydrogenation to formate and methanol as an alternative to photo- and electrochemical CO_2 reduction, Chem. Rev. 115 (2015) 12936–12973.
[25] T.A. Manes, M.J. Rose, Redox properties of a bis-pyridine rhenium carbonyl derived from an anthracene scaffold, Inorg. Chem. Commun. 61 (2015) 221–224.
[26] N.M. Rezayee, C.A. Huff, M.S. Sanford, Tandem amine and ruthenium-catalyzed hydrogenation of CO_2 to methanol, J. Am. Chem. Soc. 137 (2015) 1028–1031.
[27] J. Huang, J. Chen, H. Gao, L. Chen, Kinetic aspects for the reduction of CO_2 and CS_2 with mixed-ligand ruthenium(ii) hydride complexes containing phosphine and bipyridine, Inorg. Chem. 53 (2014) 9570–9580.
[28] C. Zúñiga, I. Crivelli, B. Loeb, Synthesis, characterization, spectroscopic and electrochemical studies of donor–acceptor ruthenium(II) polypyridine ligand derivatives with potential NLO applications, Polyhedron 85 (2015) 511–518.
[29] A. Carreño, M. Gacitúa, E. Schott, X. Zarate, J.M. Manriquez, M. Preite, S. Ladeira, A. Castel, N. Pizarro, A. Vega, I. Chavez, R. Arratia-Perez, Experimental and theoretical studies of the ancillary ligand (*E*)-2-((3-amino-pyridin-4-ylimino)-methyl)-4,6-di-*tert*-butylphenol in the rhenium(I) core, New J. Chem. 39 (2015) 5725–5734.
[30] M.-N. Collomb-Dunand-Sauthier, A. Deronzier, R. Ziessel, Electrochemical elaboration of thin films of poly[$Ru^{II}(L)(CO)_2Cl_2$] (L = 4-(2-pyrrol-1-ylethyl)-4'-methyl-2,2'-bipyridine or 4,4'-bis((3-pyrrol-1-ylpropyloxy)carbonyl)-2,2'-bipyridine): photochemical properties and photoimaging, J. Phys. Chem. 97 (1993) 5973–5979.
[31] G. Gerbaud, J.M. Mouesca, S. Hediger, S. Chardon-Noblat, F. Lafolet, A. Deronzier, M. Bardet, Structural characterization of metal–metal bonded polymer $[Ru(L)(CO)_2]_n$ (L = 2,2′-bipyridine) in the solid state using high-resolution NMR and DFT chemical shift calculations, Phys. Chem. Chem. Phys. 12 (2010) 15428–15435.
[32] D. Oyarzún, R. Córdova, O.E. Linarez Pérez, E. Muñoz, R. Henriquez, M. López Teijelo, H. Gomez, J. Solid State Electrochem. 15 (2011) 2265–2275.
[33] A. Deronzier, Conducting polymers and polymer electrolytes: from biology to photovoltaics, Editor ACS Sym. Ser. 832 (2003) 141.
[34] M.-N. Collomb, A. Deronzier, R. Ziessel, Electrocatalytic reduction of carbon dioxide with mono(bipyridine)carbonylruthenium complexes in solution or as polymeric thin films, Inorg. Chem. 33 (1994) 2961–2967.
[35] F.C. Krebs, H. Spanggaard, Significant improvement of polymer solar cell stability, Chem. Mater. 17 (2005) 5235–5237.
[36] J.-F. Yin, D. Bhattacharya, Y.-C. Hsu, C.-C. Tsai, K.-L. Lu, H.-C. Lin, J.-G. Chen, K.-C. Ho, Enhanced photovoltaic performance by synergism of light-cultivation and electronic localization for highly efficient dye-sensitized solar cells, J. Mater. Chem. 19 (2009) 7036–7042.
[37] S. Wenger, P.A. Bouit, Q. Chen, J. Teuscher, D.D. Censo, R. Humphry-Baker, J.E. Moser, J.L. Delgado, N. Martin, S.M. Zakeeruddin, M. Grätzel, Efficient electron transfer and sensitizer regeneration in stable π-extended tetrathiafulvalene-sensitized solar cells, J. Am. Chem. Soc. 132 (2010) 5164–5169.
[38] S. Chardon, A. Deronzier, R. Ziessel, D. Zsoldos, Electroreduction of CO_2 catalyzed by polymeric $[Ru(bpy)(CO)_2]_n$ films in aqueous media: parameters influencing the reaction selectivity, J. Electroanal. Chem. 444 (1998) 253–260.
[39] D. Oyarzún, O. Linarez Pérez, M. López Teijelo, C. Zúñiga, E. Jeraldo, D. Geraldo, R. Arratia-Perez, Mater. Lett. 165 (2016) 67–70.
[40] S. Umapathy, G. Lee-Son, R.E. Hester, Raman spectroscopic studies of substituted bipyridines, their ruthenium(II) complexes and surface-derivatized TiO_2, J. Molec. Sctruct. 194 (1989) 107–116.
[41] Jun Wang, Lei Zhao, Victor S.-Y. Lin, Zhiqun Lin, Formation of various TiO_2nanostructures from electrochemically anodized titanium, J. Mater. Chem. 19 (2009) 3682–3687.
[42] S. Umapathy, G. Lee-Son, R.E. Hester, Resonance Raman spectroscopic studies of surface-derivatized TiO_2, J. Chem. Soc. Chem. Commun. 24 (1987) 1841–1842.
[43] T.V. Magdesieva, I.V. Zhukov, D.N. Kravchuk, O.A. Semenikhin, L.G. Tomilova, K. P. Butin, Electrocatalytic CO_2 reduction in methanol catalyzed by mono, di, and electropolymerized phthalocyanine complexes, Russ. Chem. Bull. Int. Ed. 51 (2002) 805–812.
[44] S. Chardon, A. Deronzier, F. Harlt, J. van Slageren, T. Mahabiersing, A novel organometallic polymer of osmium(0), [Os(2,2′-bipyridine)$(CO)_2$]*n*: Its electrosynthesis and electrocatalytic properties towards CO_2 reduction, Eur. J. Inorg. Chem. (2001) 613–617.